

Enhanced piezoelectricity in ABO_3 ferroelectrics via intrinsic stress-driven flattening of the free-energy profile

Yu Feng,^{1,2} Wei-Li Li,^{1,3} Yang Yu,¹ He-Nan Jia,¹ Yu-Long Qiao,¹ and Wei-Dong Fei^{1,4,*}

¹*School of Materials Science and Engineering, Harbin Institute of Technology, Harbin 150001, People's Republic of China*

²*Key Laboratory of Engineering Dielectrics and Its Application, Ministry of Education, Harbin University of Science and Technology, Harbin 150080, People's Republic of China*

³*National Key Laboratory of Science and Technology on Precision Heat Processing of Metals, Harbin Institute of Technology, Harbin 150001, People's Republic of China*

⁴*State Key Laboratory of Advanced Welding and Joining, Harbin Institute of Technology, Harbin 150001, People's Republic of China*
(Received 19 August 2016; revised manuscript received 9 November 2016; published 17 November 2017)

An approach to greatly enhance the piezoelectric properties (~ 400 pC/N) of the tetragonal $BaTiO_3$ polycrystal using a small number of A -site acceptor-donor substitutions [D. Xu *et al.*, *Acta Mater.* **79**, 84 (2014)] has been proposed. In this study, $Pb(ZrTi)O_3$ (PZT) based polycrystals with various crystal symmetries (tetragonal, rhombohedral, and so on) were chosen to investigate the piezoelectricity enhancement mechanism. X-ray diffraction results show that doping generates an intrinsic uniaxial compressive stress along the $[001]_{pc}$ direction in the ABO_3 lattices. Piezoelectric maps in the parameter space of temperature and Ti concentration in the PZT and doped system show a more significant enhancement effect of $Li^+ - Al^{3+}$ codoping in tetragonal PZT than in the rhombohedral phase. Phenomenological thermodynamic analysis indicates that the compressive stress results in more serious flattening of the free-energy profile in tetragonal PZT, compared with that in the rhombohedral phase. The chemical stress obtained by this acceptor-donor codoping can be utilized to optimize the piezoelectric performance on the tetragonal-phase site of the morphotropic phase boundary in the PZT system. The present study provides a promising route to the large piezoelectric effect induced by chemical-stress-driven flattening of the free-energy profile.

DOI: [10.1103/PhysRevMaterials.1.064405](https://doi.org/10.1103/PhysRevMaterials.1.064405)

I. INTRODUCTION

Acceptor doping, donor doping, and acceptor-donor codoping in metal oxides and ABO_3 systems have been investigated intensively [1–9]. Acceptor doping and donor doping will cause the ferroelectric characteristics of piezoelectrics to be “hard” and “soft,” respectively [10,11]. The acceptor or donor substitutions in the ABO_3 systems will result in the formation of defect dipoles between the substitutions and vacancies (oxygen or cation vacancies). In order to reduce the probability of vacancies, acceptor-donor codoping in the same sites is proposed as a universal strategy that can be applied to ABO_3 -type ferroelectric materials. In fact, the A -site or B -site acceptor-donor codoping has been researched, such as $BaTiO_3$ -(NaBi), $BaTiO_3$ -(MnNb), and so on [4–6,8,12]. However, early works even led some researchers to suggest that such doping might have little effect on the piezoelectric performance.

Recently, Yao *et al.* found that $BaTiO_3$ ceramics doped by Na^+ / Er^{3+} cosubstituting at the A site possessed excellent piezoelectric properties (piezoelectric coefficient, electromechanical coupling factor, and mechanical quality factor) [13]. With increasing Na^+ and Er^{3+} concentration, the lattice parameter and unit cell volume will be reduced because of the smaller radii of Na^+ and Er^{3+} . Our recent research has indicated that the replacement of Ba^{2+} by the smaller Li^+ and Al^{3+} ions at A sites can also improve the piezoelectric properties of $BaTiO_3$ -based ceramics [14,15]. Higher piezoelectric proper-

ties ($d_{33} = 378$ pC/N) were found in the $BaTiO_3$ ceramics doped by $LiAlSiO_4$. It is suggested that Li^+ , Al^{3+} , and Si^{4+} substitute at the A , A , and B sites, respectively [14]. With increasing $LiAlSiO_4$ concentration, the lattice parameter (c) and tetragonality significantly decreased, which was consistent with the results given in the $Ba(NaEr)TiO_3$ system [13]. In order to research the effect of A -site substitution (Li^+ and Al^{3+}) rather than B -site substitution (Si^{4+}) on the piezoelectric properties of $BaTiO_3$, stoichiometric $Ba_{1-2x}Li_xAl_xTiO_3$ (BLAT for short) ceramics were fabricated via a conventional solid state reaction, and the piezoelectric properties were investigated. Both high d_{33} (>300 pC/N) and huge Q_m (>2000) were obtained in the tetragonal $Ba_{0.98}Li_{0.01}Al_{0.01}TiO_3$ ceramic. This demonstrates that this system is a potential candidate for lead-free piezoelectric materials in high-power applications [15]. Besides, the ferroelectric and piezoelectric properties of PZT(52/48) ceramics doped by Li^+ and Al^{3+} were investigated. Doping can also enhance the piezoelectric properties of PZT(52/48) ceramics [16]. The effect of A -site substitutions (Li^+ and Al^{3+}) on the enhanced piezoelectric performance of $BaTiO_3$ and PZT(52/48) is confirmed to be significant.

It is well known that the intrinsic and extrinsic components can contribute to the enhanced piezoelectric response in piezoelectric ceramics [17–20]. Large piezoelectric effect in ABO_3 piezoelectrics is generally related to the morphotropic phase boundary (MPB) or polymorphic phase transition (PPT) [21–25]. However, the excellent piezoelectric properties of $BaTiO_3 / LiAlSiO_4$ or BLAT ceramics do not result from intrinsic components—the MPB or PPT—because there is no coexistence of two or more phases in the doped ceramics.

*Corresponding author: wdfei@hit.edu.cn

Meanwhile, the extrinsic components related to the nanodomain structures and/or submicron grain can also be ruled out [15,26]. Although a mechanism for local low symmetry induced by Li^+ - Al^{3+} pairs has been proposed in our previous works, there is a noticeable lack of comprehensive mechanisms for this piezoelectric enhancement in BaTiO_3 and PZT systems [14–16].

It is shown that on the thermodynamic phenomenological level, the common origin of the piezoelectric enhancement and its anisotropy in perovskites is the flattening of a free-energy profile. First-principles calculation studies have shown a correlation between the flattening of a free-energy profile and enhanced piezoelectric response in ferroelectrics as the fundamental mechanism [27]. The origins of the strong piezoelectric response observed in $(\text{KNa})\text{NbO}_3$ (KNN), PZT, and $(\text{BaCa})\text{TiO}_3$ - $\text{Ba}(\text{ZrTi})\text{O}_3$ (BCT-BZT) are reported to be the PPT, MPB, and tricritical triple point (TCP), respectively [28–31]. The above mechanisms are related to phase instability, which results in the flattening of a free-energy profile and reduced energy barrier. Finally, exceptional piezoelectric properties are obtained near phase boundaries. The PPT, MPB, and TCP can be achieved via regulation of composition. Thus, they are regarded as the method termed “compositionally driven flattening of a free-energy profile” [32–40]. Besides, electrical, mechanical, and temperature fields can also affect the anisotropy of the energy surface because free energy is a function of these fields [41–47].

Lead zirconate-titanate is by far the most common piezoelectric material for actuator, transducer, and sensor applications. The crystal structure of $\text{PbZr}_x\text{Ti}_{1-x}\text{O}_3$ changes from the tetragonal (*T*) to rhombohedral (*R*) phase via an intermediary monoclinic (*M*) phase as *x* increases from 0 to 1 [31]. In this study, PZT ceramics with different crystal symmetries (*T*, *M*, and *R*) were chosen to investigate the piezoelectricity enhancement mechanism of *A*-site acceptor-donor codoping. X-ray diffraction (XRD) results reveal the effect of the dopant on the crystal structure and lattice distortion in the PZT system. The lattice distortion can be regarded as a result induced by chemical stress because of the radius difference between Pb^{2+} and the substitutions [48]. In the framework of the Landau-Ginzburg-Devonshire (LGD) theory, the enhanced properties of tetragonal BLAT and PLAZT ceramics are related to the stress-driven flattening of a free-energy profile. The piezoelectric properties show that the stress-driven piezoelectric enhancement can be superimposed on the compositionally driven one (MPB). The special chemical stresses can cause flattening of a free-energy profile in the piezoelectric system, which then results in a large piezoelectric response.

II. EXPERIMENTAL

A. Materials and the preparation of PZT and PLAZT ceramics

Stoichiometric $\text{PbZr}_x\text{Ti}_{1-x}\text{O}_3$ and $\text{Pb}_{0.98}\text{Li}_{0.01}\text{Al}_{0.01}\text{Zr}_x\text{Ti}_{1-x}\text{O}_3$ (PLAZT for short) with Zr/Ti ratio of 60/40, 55/45, 53/47, 52/48, and 45/55 were fabricated via conventional solid state reaction using Pb_2O_3 , ZrO_2 , TiO_2 , Li_2O , and Al_2O_3 ($\geq 99.9\%$, Aladdin Chemistry Co. Ltd, Shanghai, China), respectively. An excess of 3 mol % Pb_2O_3 was included to compensate for Pb loss

during sintering. The starting reagents were ball milled in ethanol for 15 h. After ball milling, the resulting slurries were dried at 80°C for 12 h, then calcined in an alumina crucible at 800°C for 2 h. The calcined powders were then ball milled in ethanol for 15 h using ZrO_2 ball-milling media, followed by drying the slurries at 80°C for 12 h. The dried powders were pressed into pellets of 10 mm in diameter and 1 mm in thickness using a few drops of 5 wt % polyvinyl alcohol (PVA) as a binder. After burning off the PVA, the PZT and PLAZT pellets embedded in the remaining powder were heated to 1200°C at a rate of $5^\circ\text{C}/\text{min}$, and then sintered at 1200°C for 2 h.

B. Characterization

Powder and ceramic XRD were carried out using a Philips X'Pert diffractometer with $\text{Cu K}\alpha$ radiation with a step size of 0.05° and 0.5 s per step. The fine-scan XRD patterns were collected with a step size of 0.02° and 5 s per step. Ag electrodes were prepared on both sides of the ceramics by annealing at 550°C for 30 min for electrical measurements. The piezoelectric coefficient (d_{33}) was measured using a quasistatic piezoelectric coefficient testing meter (ZJ-4AN, Institute of Acoustics, Chinese Academy of Science). The dielectric property measurements of every sample were carried out via an Agilent 4294A impedance analyzer. The electromechanical coupling coefficient (k_p) was determined by the resonance-antiresonance method on the basis of IEEE standards using an Agilent 4294A impedance analyzer [49]. The thermal stabilities of d_{33} and k_p were measured via separate *ex situ* thermal depolarization measurements. The measurements were completed in which the samples were annealed at a set temperature for 30 min in a furnace, after which they were removed and the d_{33} and k_p were measured [50].

III. RESULTS AND DISCUSSION

A. Phase characterization

Figure 1 shows the XRD patterns of PZT and PLAZT powders with $\text{Zr}/\text{Ti} = 60/40, 55/45, 53/47, 52/48, \text{ and } 45/55$ in the 2θ range of 20° – 80° measured at room temperature. All diffraction peaks match well the ABO_3 -type perovskite phase without additional phases. In order to investigate the effect of doping on the PLAZT lattice, fine-scan XRD was performed at room temperature for the PZT and PLAZT powders, and the patterns are shown in Figs. 2(a)–2(e). Every fine-scan XRD pattern includes $\{110\}$, $\{111\}$, and $\{200\}$ reflections (indexed in pseudocubic coordinates). The location of every PZT sample with different Zr/Ti ratios at room temperature has been marked in the phase diagram of the PZT system as shown in Fig. 2(f) [22].

Figure 2(a) presents the $\{110\}$, $\{111\}$, and $\{200\}$ reflections of PZT(60/40) and PLAZT(60/40). The diffraction data confirm that both PZT(60/40) and PLAZT(60/40) exhibit rhombohedral crystal symmetry, as evidenced by the relative intensity ratios of the $\{110\}$ and $\{111\}$ reflections and the existence of a single $\{200\}$ peak. For every $\{110\}$ and $\{111\}$ peak, the location and shape are almost unchanged after

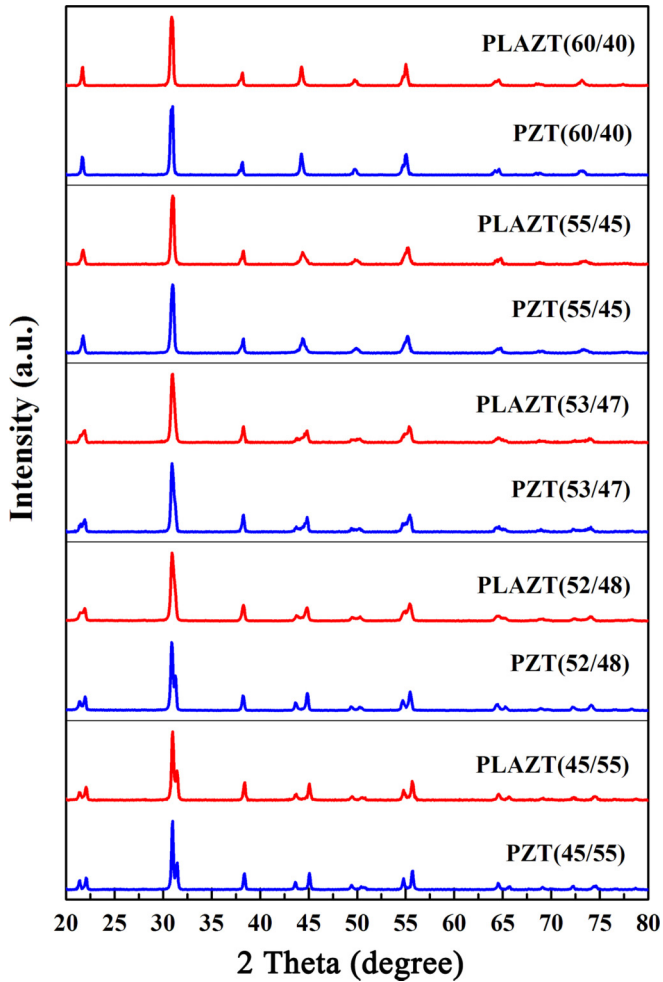


FIG. 1. XRD patterns of PZT and PLA ZT powders with different Zr/Ti ratios (60/40, 55/45, 53/47, 52/48, and 45/55) in the 2θ range of 20° – 80° measured at room temperature.

doping. The effect of doping on the crystal symmetry of rhombohedral PZT(60/40) is little.

Figure 2(b) presents the $\{110\}$, $\{111\}$, and $\{200\}$ reflections of PZT(55/45) and PLA ZT(55/45). It is clear that the $\{111\}$ reflections of PZT(55/45) and PLA ZT(55/45) should be fitted via three peaks. In addition, the $\{200\}$ reflections are not single-peaked. The above results indicate that the crystal symmetries of PZT(55/45) and PLA ZT(55/45) are not single rhombohedral phases. Considering the location of PZT(55/45) in the phase diagram of the PZT system as shown in Fig. 2(f), local rhombohedral and monoclinic crystal lattices possibly coexist in PZT(55/45) at room temperature [22,51,52]. Compared with the $\{111\}$ reflection of PZT(55/45), doping makes the characteristics of the three peaks in the $\{111\}$ reflection of PLA ZT(55/45) more obvious [30]. The above differences confirm that there are more monoclinic crystal lattices in PLA ZT(55/45).

Figure 2(c) presents the $\{110\}$, $\{111\}$, and $\{200\}$ reflections of PZT(53/47) and PLA ZT(53/47). It is clear that both the $\{111\}$ and $\{200\}$ reflections of PZT(53/47) and PLA ZT(53/47) should be fitted via three peaks. Based on the location of PZT(53/47) in the phase diagram of the PZT

system as shown in Fig. 2(f), the diffraction data confirm that both PZT(53/47) and PLA ZT(53/47) exhibit monoclinic crystal symmetry [31]. After doping, the (101) and (200) peaks shift towards the (110) and (002) peaks, respectively. The distances between the two obvious peaks in the $\{110\}$ and $\{200\}$ reflections are reduced after doping, which indicates that doping reduces the axis ratio c/a .

The $\{110\}$, $\{111\}$, and $\{200\}$ reflections of PZT(52/48) and PLA ZT(52/48) are shown in Figs. 2(d1), 2(d2), and 2(d3), respectively. According to the location of PZT(52/48) in the phase diagram and the XRD results, local tetragonal and monoclinic crystal lattices possibly coexist in PZT(52/48). After doping, two peaks in the $\{200\}$ reflections of PLA ZT(52/48) move towards each other, which suggests that the axis ratio is reduced [similarly to that observed in Fig. 2(c3)]. The variations should be attributed to the decrease in lattice parameter c because the locations of the (110) and (200) peaks are almost unchanged compared with the (101) and (002) peaks. In addition, the large $\{111\}$ reflection in PLA ZT(52/48) confirms that there may be a small number of tetragonal crystal lattices transferring to monoclinic crystal lattices after doping.

The $\{110\}$, $\{111\}$, and $\{200\}$ reflections of PZT(45/55) and PLA ZT(45/55) are shown in Figs. 2(e1), 2(e2), and 2(e3), respectively. The diffraction data confirm that both PZT(45/55) and PLA ZT(45/55) exhibit tetragonal symmetry, as evidenced by the relative intensity ratios of the (002)/(200) and the existence of a single (111) peak at $2\theta = 38.36^\circ$. The right shift of the (111) peak for PLA ZT(45/55) is observed in Fig. 2(e2), as the small ionic radii of Li^+ and Al^{3+} at the A sites compared with Pb^{2+} cause a slight reduction in the lattice parameters, which once again confirms that Li^+ and Al^{3+} are entering the PZT matrix. It is worth noting that doping affects the characteristics of the (002) peak rather than the (200) peak, which is also observed in Fig. 2(d3). For the (200) peak, the location and shape are almost unchanged in PLA ZT(45/55). For the (002) peak, there are obvious variations in the location and shape after doping. The lattice parameter c decreases after doping, which is similar to that observed in PLA ZT(52/48). The tetragonality reduction here is different from that induced by changing the Zr/Ti ratio because an increase in a will follow the decreased c in the course of increasing the Zr/Ti ratio. In order to determine whether the shift of the paraelectric-ferroelectric phase transition boundary occurs after doping, the Curie temperatures of PZT and PLA ZT ceramics have been measured and shown in Fig. 2(f). The Curie temperatures of PLA ZT with various Zr/Ti ratios are almost the same as those of the corresponding PZT. Thus, the variation of the lattice parameter c observed in PLA ZT(52/48) and PLA ZT(45/55) is possibly due to the local lattice distortion rather than the shift of the phase diagram. In addition, an obvious variation in the relative intensity ratio of the (002)/(200) peaks (I_{002}/I_{200}) is observed in Fig. 2(e3) for PLA ZT(45/55) after doping. The standard value of I_{002}/I_{200} for PZT(45/55) is about 0.5, while that for PLA ZT(45/55) is just 0.42. Besides, the tetragonality comparison between PZT(53/47, 52/48, 45/55) and PLA ZT(53/47, 52/48, 45/55) is shown in Fig. 2(g). The tetragonality in both tetragonal and nontetragonal systems is calculated using the axis ratio c/a . The tetragonality for PLA ZT is lower than that for the corresponding PZT, which indicates that doping mainly results in the reduction of the lattice parameter c .

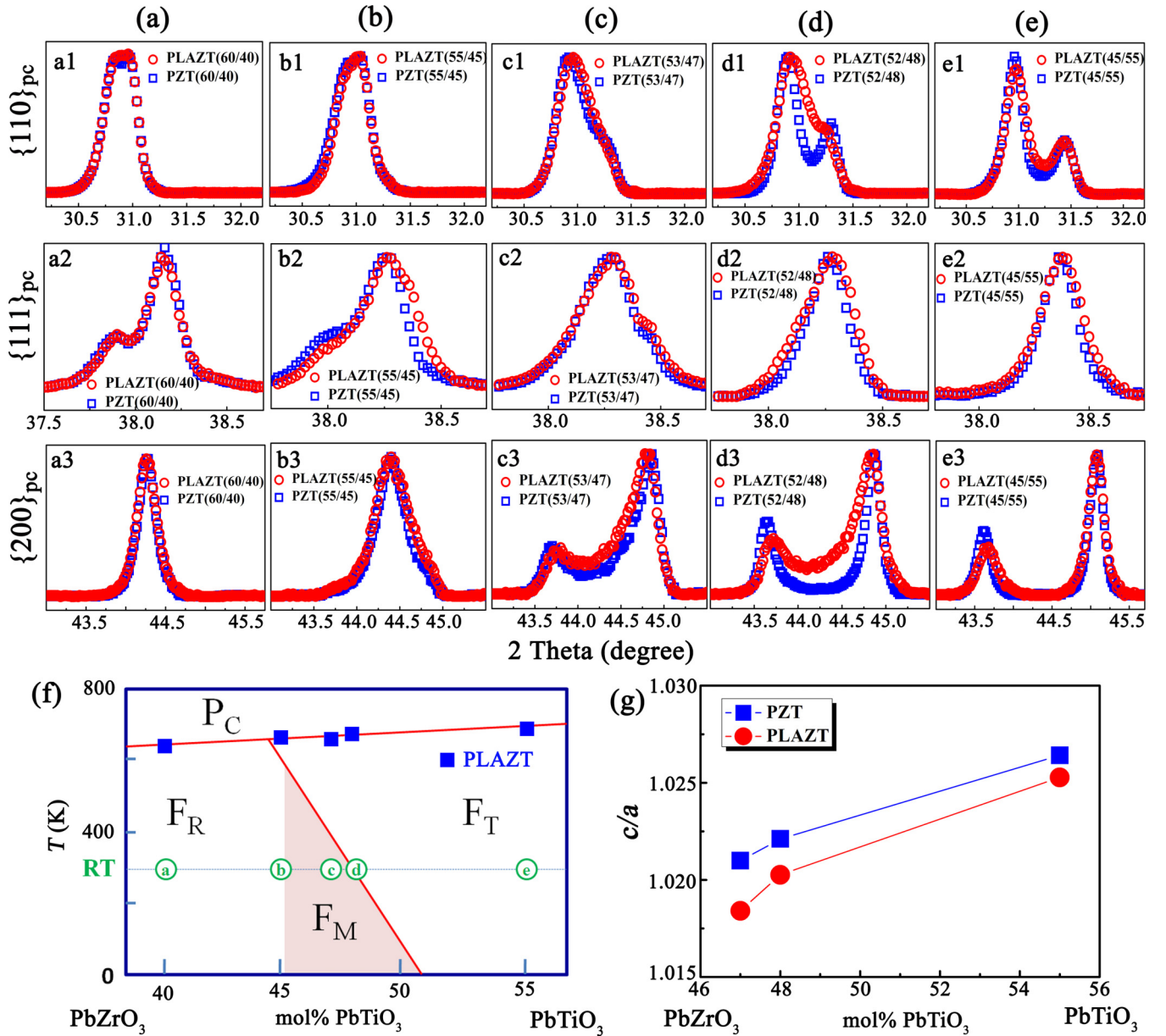


FIG. 2. Fine-scan XRD patterns of (a) PZT(60/40) and PLA-ZT(60/40), (b) PZT(55/45) and PLA-ZT(55/45), (c) PZT(53/47) and PLA-ZT(53/47), (d) PZT(52/48) and PLA-ZT(52/48), (e) PZT(45/55) and PLA-ZT(45/55). Every fine-scan XRD pattern includes $\{110\}$, $\{111\}$, and $\{200\}$ reflections of PZT and PLA-ZT. (f) The location of measured samples in the phase diagram of the PZT system at room temperature. The T - M phase transition line is from Ref. [31]. The Curie line is based on our measured dielectric spectra of PZT ceramics. The a, b, c, d, and e represent the location of PZT(60/40), (55/45), (53/47), (52/48), and (45/55) in the phase diagram of the PZT system, respectively. (g) Tetragonal comparison between PZT (53/47, 52/48, 45/55) and PLA-ZT (53/47, 52/48, 45/55).

Due to the smaller ionic radii of Li^+ and Al^{3+} as compared to Ba^{2+} , the presence of Li^+ and Al^{3+} will induce a local lattice distortion into the PZT lattice, thus reducing the diffracted intensity of x rays in the distorted direction. Considering the results in Figs. 2(e3) and 2(g), lattice distortion induced by doping has little impact on the diffracted intensity of the (200) plane, but weakens the diffracted intensity of the (002) plane. Under these circumstances, the lattice distortion, induced by acceptor-donor substitutions, mainly occurs along the $[001]_{pc}$ direction. Therefore, I_{002} decreases more quickly than I_{200} , and I_{002}/I_{200} is reduced [14,15].

B. Piezoelectric coefficient and electromechanical coupling coefficient

The d_{33} and k_p measurements of all PZT and PLA-ZT samples at room temperature are carried out, and shown in Figs. 3(a) and 3(b), respectively. With an increase in Ti content, the crystal symmetry of PZT passes through the R phase, into the M phase, and finally to the T phase [22]. During this process, both the d_{33} and k_p of PZT first increase (R - M) and then decrease (M - T). For PZT, the largest d_{33} (265 pC/N) and k_p (0.56) are observed in PZT(52/48) and PZT(53/47), respectively. The most excellent properties are found near the

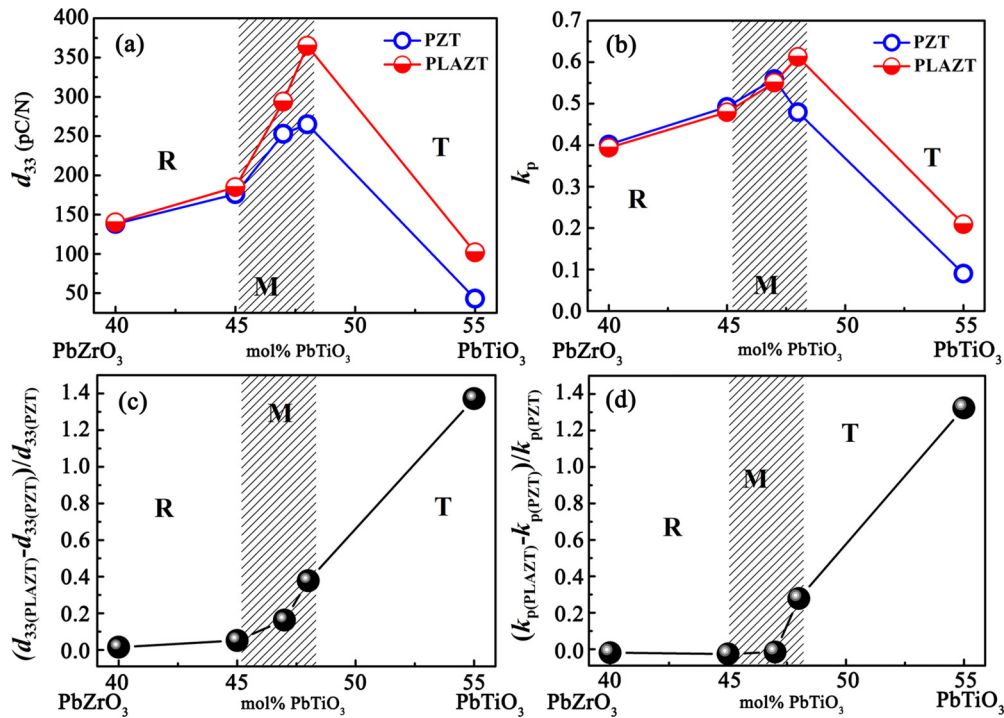


FIG. 3. d_{33} (a) and k_p (b) as a function of $PbTiO_3$ content in PZT and PLAzt. Growth rate of d_{33} (c) and k_p (d) as a function of $PbTiO_3$ content in PLAzt. The composition range of the M region is obtained from Ref. [31].

MPB and in the M region, respectively. The trends of d_{33} and k_p in PLAzt with Ti content are similar to those in PZT. The largest values of d_{33} (365 pC/N) and k_p (0.61) are both obtained in PLAzt(52/48). Obviously, doping brings different effects on the piezoelectric properties of PZT ceramics with various symmetries. By contrasting and analyzing the above results, the growth rates of d_{33} and k_p in PLAzt are shown in Figs. 3(c) and 3(d), respectively. Doping enhances the piezoelectric performance of PZT(45/55) and PZT(52/48) rather than PZT(53/47), PZT(55/45), or PZT(60/40). In other words, acceptor-donor substitutions at the A site will bring positive effects on the piezoelectric properties of PZT ceramics with the T and $T+M$ phases.

The d_{33} values of PZT and PLAzt are plotted as a function of temperature in Fig. 4(a). The temperature stability of d_{33} in PLAzt with various compositions is similar to that in PZT. There is no obvious depolarization in PZT or PLAzt with increasing temperature. The enhanced effect of doping on the d_{33} of PLAzt(52/48) and PLAzt(45/55) continues to their Curie temperatures. The contour plots of d_{33} in PZT and PLAzt as a function of temperature and composition are shown in Figs. 4(b) and 4(c), respectively. The excellent d_{33} values for PZT are observed along the M to T phase boundary in the range of $52/48 \leq Zr/Ti \leq 54/46$. The two-dimensional flattening of the energy profile (polarization rotation and polarization extension/contraction) is responsible for the exceptionally large piezoelectric coefficient in the temperature range of 475–650 K [53–55]. The largest d_{33} values for PLAzt as shown in Fig. 4(c) emerge from the M to T phase boundary in the range of $49/51 \leq Zr/Ti \leq 54/46$, continuing up to the convergence region with a higher degree of tilting than predicted by the phase boundary. The contour

plot of d_{33} in PLAzt predicts that excellent piezoelectric coefficients will be obtained in a relatively wide composition range ($49/51 \leq Zr/Ti \leq 54/46$).

The k_p values of PZT and PLAzt as a function of temperature are presented in Fig. 5(a). The temperature stability of k_p in PLAzt with various compositions is similar to that in PZT. Differing from d_{33} , k_p gradually decreases as the temperature approaches the Curie temperature. The contour plots of k_p in PZT and PLAzt as a function of temperature and composition are shown in Figs. 5(b) and 5(c), respectively. The highest k_p (~ 0.6) for PZT are observed in the M region and along the M to T phase boundary in the range of $52/48 \leq Zr/Ti \leq 54/46$, which is in agreement with the d_{33} results as shown in Fig. 4(b). The largest k_p values for PLAzt, as shown in Fig. 5(c), emerge along the M to T phase boundary in the range of $49/51 \leq Zr/Ti \leq 54/46$, elongating into part of the T region. The composition range ($49/51 \leq Zr/Ti \leq 54/46$) of the excellent k_p values for PLAzt occurring in Fig. 5(c) is the same as that of the d_{33} values as shown in Fig. 4(c). The contour plot of k_p in PLAzt predicts that the enhanced k_p can also be obtained in a relatively wide composition range ($49/51 \leq Zr/Ti \leq 54/46$) compared with that ($52/48 \leq Zr/Ti \leq 54/46$) in PZT.

As expected, it is clearly observed in Figs. 3, 4(b), and 5(b) that the piezoelectric properties of PZT are maximized in the M region or near the MPB, which is consistent with previous studies [56]. When a small number of acceptor-donor ions substitute at the A site, the piezoelectric properties of PLAzt with the T or $T+M$ phase are largely enhanced as shown in Figs. 3, 4(c), and 5(c). Combined with the XRD patterns as shown in Fig. 2, this doping can largely affect the tetragonal crystal symmetry and the corresponding

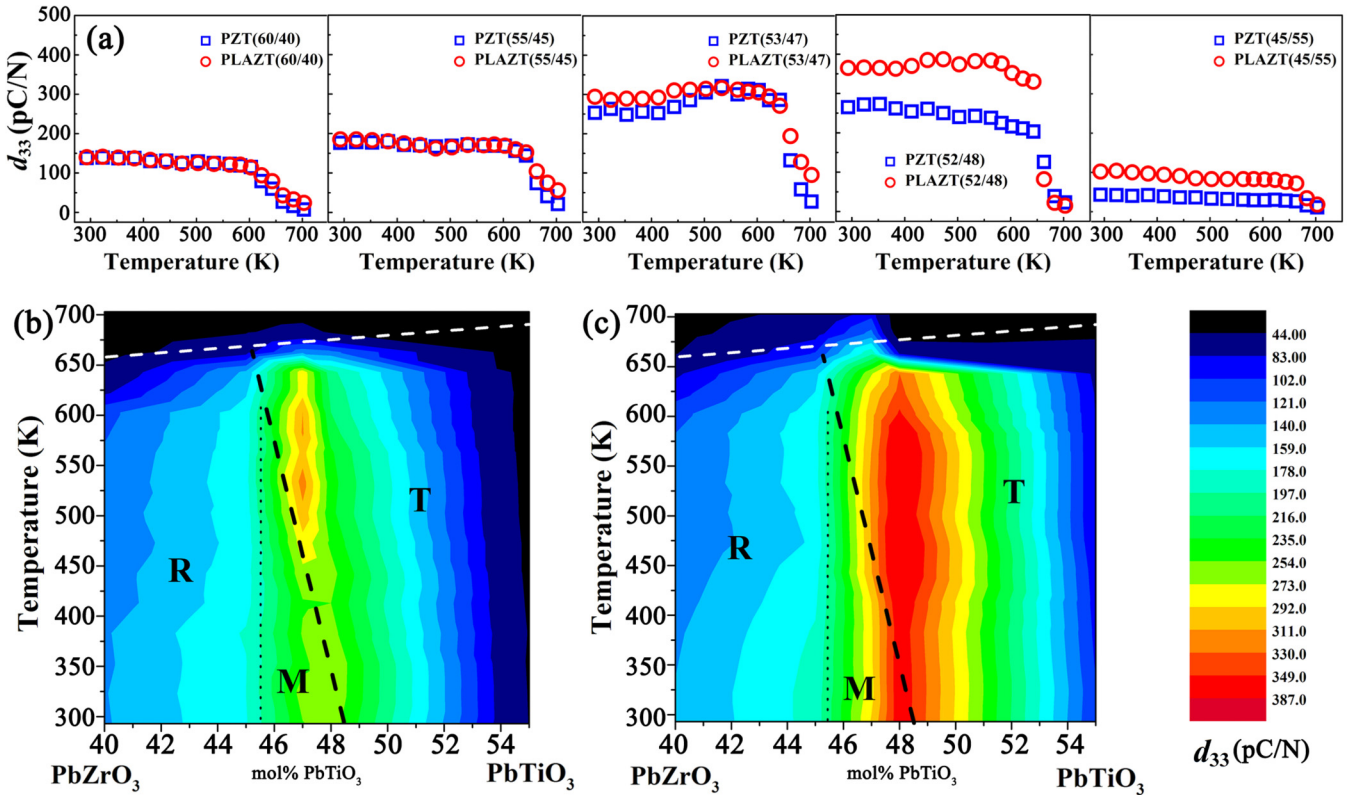


FIG. 4. d_{33} of PZT and PLAZT for Zr/Ti ratio from 60/40 to 45/55 as a function of temperature (a). Contour plot of d_{33} as a function of temperature and composition in PZT (b) and PLAZT (c). The white dashed line indicates the Curie line obtained from our measured dielectric spectra. The black dashed and dotted lines indicate the M - T and M - R lines obtained from Ref. [31]. The variation of properties between the measured points was estimated by linear interpolation between them.

piezoelectric properties. For the rhombohedral lattices, doping has little effect on their properties. Further experiments and calculations are carried out to determine the physical origins of these observations.

C. Distribution of acceptor-donor ions and lattice distortion

The above XRD results show that lattice distortion mainly occurs along the $[001]_{pc}$ direction, showing the reduction of the lattice parameter c and I_{002}/I_{200} . This would mean that doping generates an intrinsic compressive stress along the $[001]_{pc}$ direction as shown in Fig. 6(a). The lattice distortion can be regarded as a result induced by chemical stress because of the radius difference between Pb^{2+} and the substitutions [48]. The stress is considered to be uniaxial because the lattice parameter a for PLAZT(45/55) is almost unchanged. However, there is still the question of creating a uniaxial stress in the polycrystal via doping. Assuming that Li^+ and Al^{3+} ions distribute randomly in all the crystal planes and occupy the A sites, the trend of the diffracted intensity of the (002) peaks will be identical to that of the (200) peaks, as a consequence of the same lattice distortion [same structure factor (F)] for the (002) and (200) diffractions [14]. The distortion will affect both the (002) and (200) reflections. The I_{002}/I_{200} will be almost unchanged. Thus, there is another reasonable explanation which is consistent with our experimental results. On the basis of the defect symmetry principle proposed by Ren *et al.* and previous papers, the uniaxial stress comes

possibly from the preferential distribution of Li^+ and Al^{3+} ions [57–61]. Li^+ and Al^{3+} ions tend to maximally constitute the defect dipole (Li^+-Al^{3+}) in the same cell in order to minimize the electrostatic energy and maintain local charge balance. Thus, the distortion has been heavily concentrated along the direction of the defect dipole (Li^+-Al^{3+}) as shown in Fig. 6(b). The Li^+ and Al^{3+} ions gradually form a defect dipole in the long-term process of sintering in which diffusion of ions is serious [14].

The (NaBi)TiO₃ system should be remembered and considered at the mention of A -site acceptor-donor codoping. Compared with preferential distribution of Li^+ and Al^{3+} , Na^+ and Bi^{3+} tend to substitute at A sites and distribute disorderly in the ABO_3 lattice. Taking BaTiO₃ as example, a detailed comparison between the BaTiO₃ ceramics doped by a small amount of (Li, Al) and (Na, Bi) has been obtained and discussed as follows. The XRD results in previous papers confirm that $Ba_{1-x}(Na_{0.5}Bi_{0.5})_xTiO_3$ ($0 \leq x \leq 0.1$) exhibits tetragonal symmetry [62–65]. The [111] peaks in the $Ba_{1-x}(Na_{0.5}Bi_{0.5})_xTiO_3$ ($0 \leq x \leq 0.1$) ceramics are shifted towards the high angle. The above two changes are also observed in the BaTiO₃ ceramics doped by (Li, Al). In other words, the variation of crystal structure in the BaTiO₃ ceramics with a small amount of (Na, Bi) is consistent with that in the BaTiO₃ ceramics with a small amount of (Li, Al) because the radii of Li^+ , Al^{3+} , Na^+ , and Bi^{3+} are smaller than that of Ba^{2+} . Therefore, we cannot think that the effect of (Na, Bi) on the crystal structure of the BaTiO₃ ceramic is different from

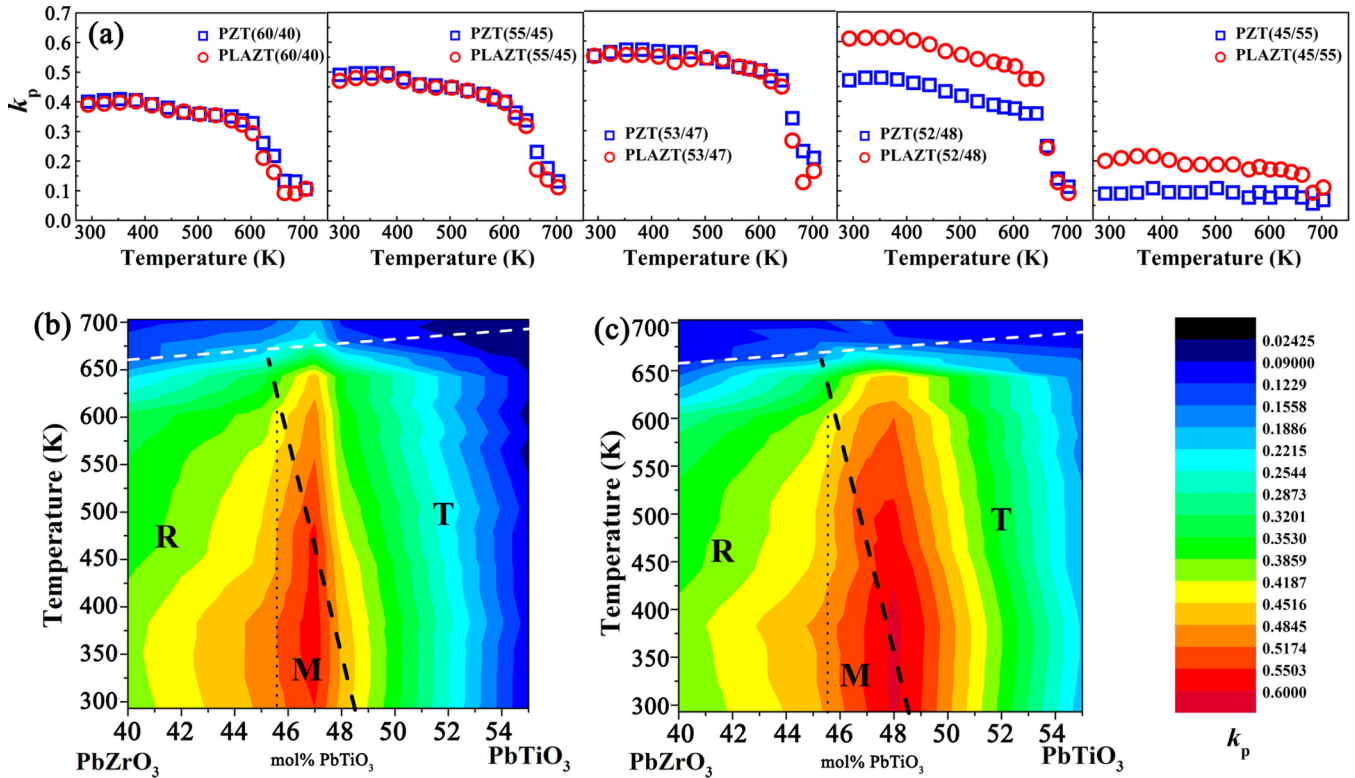


FIG. 5. k_p of PZT and PLAzt for Zr/Ti ratio from 60/40 to 45/55 as a function of temperature (a). The k_p values are obtained from resonance-antiresonance data. Contour plot of k_p as a function of temperature and composition in PZT (b) and PLAzt (c). The white dashed line indicates the Curie line obtained from our measured dielectric spectra. The black dashed and dotted lines indicate the M - T and M - R lines obtained from Ref. [31]. The variation of properties between the measured points was estimated by linear interpolation between them.

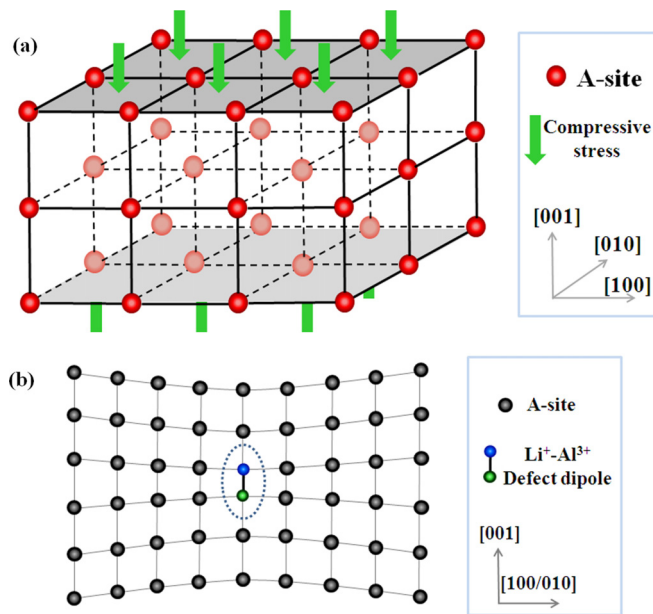


FIG. 6. Schematic illustration of compressive stress applied along the $[001]_{pc}$ direction (a). The arrows show the direction of compressive stress induced by A -site substitutions. Schematic illustration of the preferential distribution of Li^+-Al^{3+} defect dipole parallel to the $[001]_{pc}$ direction (b). The effect of compressive stress induced by Li^+-Al^{3+} defect dipole on the diffracted intensity and interplanar spacing of (200) and (002) planes.

that of (Li, Al). However, it should be noted that there are two major differences between (Li, Al) and (Na, Bi).

First, according to the classification proposed by Setter and Cross, the ordering of composite substitutions possibly exists in complex perovskite compounds with composite substitution [66,67]. It has been revealed theoretically and experimentally that the larger the ion charges and size difference between the two substitutions, the easier the two substitutions' ordering can be formed [68,69]. For ion charges, the form of (Li, Al) is the same as that of (Na, Bi) (monovalent cation and trivalent cation). However, the radius of Na^+ ($R[Na^+] = 1.16 \text{ \AA}$) is almost identical to that of Bi^{3+} ($R[Bi^{3+}] = 1.17 \text{ \AA}$). The radius of Al^{3+} ($R[Al^{3+}] = 0.67 \text{ \AA}$) is far less than that of Li^+ ($R[Li^+] = 0.90 \text{ \AA}$) [70]. Therefore, the probability of ordering for the (Li-Al) ions is larger than that for the (Na-Bi) ions. Second, the radius of $(Li_{0.5}Al_{0.5})^{2+}$ is far smaller than that of $(Na_{0.5}Bi_{0.5})^{2+}$. The local lattice distortion induced by $(Li_{0.5}Al_{0.5})^{2+}$ should be larger than that induced by $(Na_{0.5}Bi_{0.5})^{2+}$. That is the reason why the $BaTiO_3$ - $(NaBi)/TiO_3$ can easily form a solid solution while only a minor content (1.5 mol %) of (Li, Al) can be doped in the $BaTiO_3$ crystals without impurity phases [71]. Preferential distribution of (Li, Al) and greater radius difference between $(Li_{0.5}Al_{0.5})^{2+}$ and A -site ions will result in the uniaxial, greater stress in the $BaTiO_3$ doped by (Li, Al). In contrast, disorder of (Na, Bi) and smaller radius difference between $(Na_{0.5}Bi_{0.5})^{2+}$ and the A -site ion possibly cause the nonuniaxial and less stress.

D. Landau-Ginzburg-Devonshire theory analysis

Ab initio and phenomenological calculations have shown that the intrinsic mechanism of the piezoelectric property enhancement in phase transition regions is the flattening of the free-energy profile [54,72]. The flattening of a free-energy profile provides easy paths for polarization to change from one state to another, which is associated with the corresponding property enhancement. According to the XRD analysis,

$$\begin{aligned}
 G = & \alpha_1(P_1^2 + P_2^2 + P_3^2) + \alpha_{11}(P_1^4 + P_2^4 + P_3^4) + \alpha_{12}(P_1^2 P_2^2 + P_2^2 P_3^2 + P_1^2 P_3^2) \\
 & + \alpha_{111}(P_1^6 + P_2^6 + P_3^6) + \alpha_{112}[P_1^4(P_2^2 + P_3^2) + P_3^4(P_1^2 + P_2^2) + P_2^4(P_1^2 + P_3^2)] + \alpha_{123}P_1^2 P_2^2 P_3^2 \\
 & - \frac{1}{2}s_{11}(\sigma_1^2 + \sigma_2^2 + \sigma_3^2) - s_{12}(\sigma_1\sigma_2 + \sigma_1\sigma_3 + \sigma_2\sigma_3) - \frac{1}{2}s_{44}(\sigma_4^2 + \sigma_5^2 + \sigma_6^2) \\
 & - Q_{11}(\sigma_1 P_1^2 + \sigma_2 P_2^2 + \sigma_3 P_3^2) - Q_{12}[\sigma_1(P_2^2 + P_3^2) + \sigma_2(P_1^2 + P_3^2) + \sigma_3(P_1^2 + P_2^2)] \\
 & - Q_{44}(P_2^2 P_3^2 \sigma_4 + P_1^2 P_3^2 \sigma_5 + P_1^2 P_2^2 \sigma_6),
 \end{aligned} \tag{1}$$

where P_i and σ_i are the polarization and stress; α_i , α_{ij} , and α_{ijk} are the dielectric stiffness and higher-order stiffness coefficients at constant stress; s_{ij} is the elastic compliance coefficient at constant polarization; and Q_{ij} is the cubic electrostrictive constant in polarization notation. For BaTiO₃, the coefficients are taken from Refs. [73] and [74]. Coefficients for the PZT system are taken from Ref. [77] (that is, Refs. [73,74,77]). The stress dependence of the elastic Gibbs free energy (G) profile with respect to spontaneous polarization for PZT(60/40), PZT(45/55), and BaTiO₃ at room temperature is shown in Fig. S1 of the Supplemental Material [78], and corresponding discussions are also presented there. The reason why the compressive stress along the [001]_{pc} direction is chosen in rhombohedral PZT(60/40) is also discussed in the Supplemental Material [78].

In order to determine the effect of compressive stress on the energy barrier between a polarization state and another, the energy barrier is calculated. The energy barrier (E_B) (only considering polarization contraction) between the ferroelectric and paraelectric phases is $E_B = G(P') - G(P)$, where $G(P')$ and $G(P)$ are the polar values in the G - P curves. P' and P can be solved using the following equation:

$$\frac{\partial G}{\partial P} = 0. \tag{2}$$

Figure 7(a) presents the curves of normalized E_B vs compressive stress for rhombohedral PZT(60/40), tetragonal PZT(45/55), and tetragonal BaTiO₃. It can be clearly seen that the E_B of rhombohedral PZT(60/40), tetragonal PZT(45/55), and tetragonal BaTiO₃ decrease with compressive stress. The normalized E_B of tetragonal PZT(45/55) will be larger than that of BaTiO₃ but smaller than that of rhombohedral PZT(60/40) if the lattice is under the same compressive stress along the [001]_{pc} direction. Based on the above prediction, the magnitude of the enhanced piezoelectric properties in BaTiO₃ should be the largest among the three samples under the same stress. The growth rate of experimental d_{33} in rhombohedral PLAzt(60/40), tetragonal PLAzt(45/55), and tetragonal BLAT is shown in Fig. 7(b) as a comparison. The d_{33} of

this doping brings the compressive stress along the [001]_{pc} direction of the ABO₃ lattice. In this section, we investigate the effect of compressive stress (σ) applied along the [001]_{pc} direction on the elastic Gibbs free energy (G) of tetragonal PZT(45/55), BaTiO₃, and rhombohedral PZT(60/40).

Using Landau-Ginzburg-Devonshire theory the elastic Gibbs free energy can be expanded as a power series of the polarization assuming isothermal conditions [40,73–76]:

PLAZT(60/40), PLAzt(45/55), and BLAT is 0.014, 1.372, and 1.580 times higher than that of the corresponding PZT and BaTiO₃ ceramics. The largest d_{33} enhancement is observed in the BLAT ceramic, while doping has little effect on the d_{33} of PLAzt(60/40). The experimental results are consistent with the calculated data shown in Fig. 7(a). Hence, the compressive stress can induce flattening of the free-energy profile in the Landau-Ginzburg-Devonshire (LGD) framework. The flattening occurs along both the polar axis and off polar axis. The effect of compressive stress on the polarization rotation of BaTiO₃ and PZT(45/55) is investigated in the Supplemental Material [78]. The uniaxial stress results in flattening of the free-energy profile (along the polar and off polar axis) in the tetragonal BaTiO₃ and PZT ceramics. In this case, the facilitated polarization contraction and polarization rotation contribute to the enhanced d_{33} in BaTiO₃ and PLAzt(45/55) ceramics [42,54].

We believe that A-site acceptor-donor codoping in this study leads to the compressive stress along the [001]_{pc} direction. Based on the phenomenological thermodynamic theory, the compressive stress results in obvious flattening of a free-energy profile and reduced E_B for the tetragonal PZT. The reduced E_B between one polarization state and another induced by doping should be responsible for the enhanced piezoelectric properties in the tetragonal PLAzt. In order to verify that the E_B of tetragonal PLAzt is reduced, the following experiment is designed and carried out. It is well known that external pressure can change the direction of spontaneous polarization and cause domain switching in the ferroelectrics. Based on the calculated results, the E_B for the T - C phase transition in PLAzt(45/55) is smaller than that in PZT(45/55). If the same external pressure is applied on PZT(45/55) and PLAzt(45/55), domain switching is more likely to occur in PLAzt(45/55) rather than PZT(45/55) because of the reduced E_B of PLAzt(45/55). The {200} reflections of PZT(45/55) without applied pressure and under different pressure are collected, respectively. Under the same experimental condition, the {200} reflections of PLAzt(45/55) are also obtained. The influences of external pressure on the I_{002}/I_{200} for PZT(45/55) and PLAzt(45/55) are then analyzed.

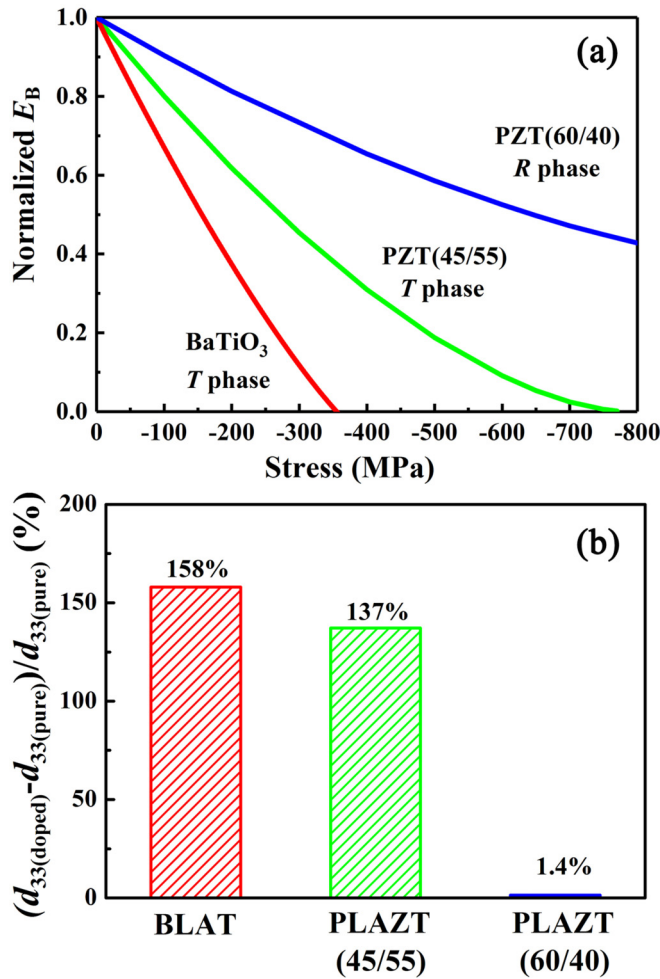


FIG. 7. Normalized E_B in PZT(60/40), PZT(45/55), and BaTiO₃ as a function of compressive stress along the $[001]_{pc}$ direction at room temperature (a). Growth rate of piezoelectric coefficient in PLA ZT(60/40), PLA ZT(45/55), and BLAT (b).

I_{002}/I_{200} as a function of external pressure applied on both sides of PZT(45/55) is shown in Fig. 8. The schematic diagram of pressure loading on PZT(45/55) is illustrated in the inset of Fig. 8. With the pressure increasing from 0 Pa to 1.4×10^5 Pa, I_{002}/I_{200} remains largely unchanged. The results indicate that the pressure of 1.4×10^5 Pa cannot change the spontaneous polarization direction in PZT(45/55) from the $[001]$ axis to the $[100]$ or $[010]$ axis. The $\{200\}$ reflections of PZT(45/55) under 0 Pa and 1.4×10^5 Pa pressure along with the fitting curves are also shown in the inset of Fig. 8.

Figure 9 presents I_{002}/I_{200} vs the pressure applied on the both sides of PLA ZT(45/55). I_{002}/I_{200} gradually increases as the pressure increases from 0 Pa to 1.4×10^5 Pa, which indicates that there is a great deal of 90° domain switching induced by external pressure. The spontaneous polarization direction in this part of the domains changes from the $[001]$ axis to the $[100]$ or $[010]$ axis. The $\{200\}$ reflections of PZT(45/55) under 0 Pa and 1.4×10^5 Pa pressure along with the fitting curves are shown in the inset of Fig. 9. Using comparative analysis of Figs. 8 and 9, we see that the domains in PLA ZT(45/55) switch more easily than those

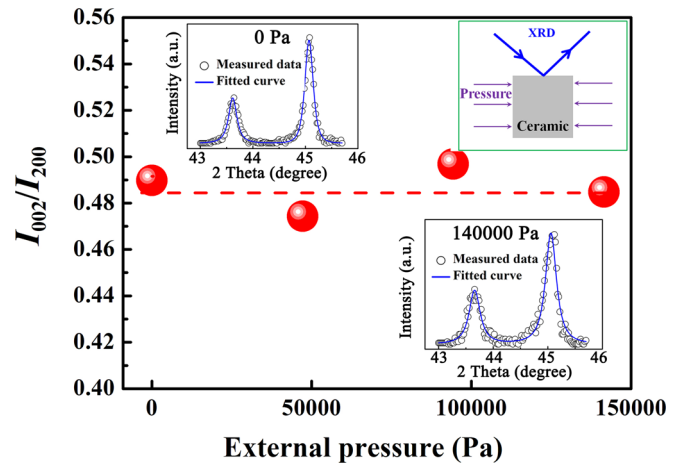


FIG. 8. I_{002}/I_{200} vs the pressure applied on both sides of PZT(45/55). The inset shows the schematic diagram of pressure loading on the PZT(45/55) and the $\{200\}$ reflections along with the fitting curves of PZT(45/55) under 0 Pa and 1.4×10^5 Pa pressure. During the peak-fitting procedure, a Pearson-VII function was used to define the profile shapes.

in PZT(45/55) under the same external pressure. It is worth noting that the aim of the comparison of Figs. 8 and Fig. 9 is only to indirectly verify the calculated result “the E_B in PLA ZT(45/55) is smaller than that in PZT(45/55).” We do not mean to calculate or compare the energy barrier of 90° domain switching in PZT and PLA ZT.

E. Stress-driven flattening of a free-energy profile in ABO_3 piezoelectrics

A-site acceptor-donor substitutions are beneficial for the piezoelectric properties of BaTiO₃, as reported in previous papers [14,15]. The systematic analyses indicate that the $Li^+ - Al^{3+}$ ions are inclined to occupy the neighboring A sites and constitute defect dipoles (ionic pairs). The larger

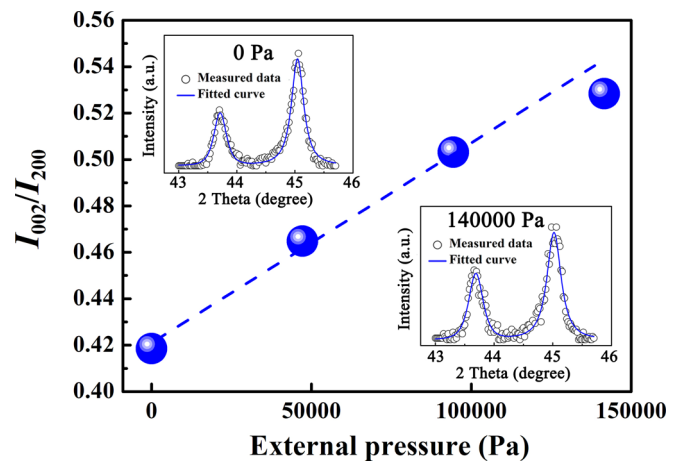


FIG. 9. I_{002}/I_{200} vs the pressure applied on both sides of PLA ZT(45/55). The inset shows the $\{200\}$ reflections along with the fitting curves of PLA ZT(45/55) under 0 Pa to 1.4×10^5 Pa pressure. During the peak-fitting procedure, a Pearson-VII function was used to define the profile shapes.

local lattice distortion will be introduced by the smaller $\text{Li}^+-\text{Al}^{3+}$ substitution at the A sites. Local low symmetry accompanying the larger local lattice distortion will appear around the $\text{Li}^+-\text{Al}^{3+}$ ionic pairs in the doped ceramics. At that time, a mechanism related to local low symmetry is proposed to explain the piezoelectric enhancement induced by this doping route in the doped BaTiO_3 ceramics. After that, this doping route was also proven to improve the piezoelectric performance of $\text{PbZr}_{0.52}\text{Ti}_{0.48}\text{O}_3$ ceramics [16]. Here piezoelectric maps in the parameter space of temperature and PbTiO_3 concentration in the PZT and doped systems show a more significant enhancement effect of $\text{Li}^+-\text{Al}^{3+}$ codoping in tetragonal PZT than in the rhombohedral phase. Based on the phenomenological thermodynamic theory, the chemical stress induced by $\text{Li}^+-\text{Al}^{3+}$ substitution can result in more obvious flattening of the free-energy profile in tetragonal PLAZT and BLAT, compared with that in rhombohedral PZT. The local low symmetry around $\text{Li}^+-\text{Al}^{3+}$ defect dipoles and the chemical stress-driven flattening of a free-energy profile should contribute to the enhanced piezoelectric enhancement in tetragonal PLAZT and BLAT systems together. The stress-driven flattening of a free-energy profile should be attributed to the special doping route and corresponding chemical stress. The piezoelectric enhancement related to this doping route does not conflict with that induced by the MPB (compositionally driven flattening of a free-energy profile). The stress- and compositionally driven flattening of a free-energy profile can be utilized to optimize the piezoelectric performance on the tetragonal-phase site of the MPB in the PZT system.

In fact, there is a great deal of published research on external pressure or electrical field tuning to the M form or MPB [79–90]. Cohen *et al.* predicted a pressure-induced anomalous phase transition and colossal enhancement of piezoelectricity in PbTiO_3 [79]. A tetragonal-to-monoclinic-to-rhombohedral-to-cubic phase transition sequence induced by external pressure and a MPB were found using first-principles theory. In the experimental works on the pressure-induced MPB in PbTiO_3 , the tetragonal-to-monoclinic-to-rhombohedral phase transition was observed at very low temperature [48]. The ambient pressure in pure PbTiO_3 is regarded as the origin of the MPB in solid solutions with PbTiO_3 . However, it seems the pressure-induced MPB in PbTiO_3 is absent at room temperature [80]. Besides, a series of studies on external pressure tuning to the M form or the MPB in the PZT system are reported [81–90]. In the Ti-rich PZT, a T - M transition was determined, but the possible M - R was not observed [81,84]. The M phase can be obtained at moderate pressure below 4 GPa for a wide range of nonmorphotropic Ti-rich PZT compositions ($20/80 < \text{Zr}/\text{Ti} < 50/50$). The above results indicate that physical pressure which acts in a similar way to “chemical pressure” can tune the M form or MPB to include nonmorphotropic compositions. In the reported work, Cohen *et al.* proposed that chemical pressure could be achieved by substituting a smaller atom for Pb in the A sites, for example $\text{Pb}_{0.5}\text{Sn}_{0.5}\text{TiO}_3$ [48]. In the present study, a kind of intrinsic, uniaxial, and compressive chemical stress is obtained in the BaTiO_3 and PZT systems via doping a few small ions. Under the intrinsic stress circumstance, tuning of the

MPB is achieved, and the composition range of the MPB is expanded.

It should be noted that the core of this idea is to obtain preferential distortion and compressive stress along a certain direction. The achievement of compressive stress should be obtained via doping smaller atom because a small radius will result in the reduction of lattice volume [48]. Besides, doping content should be limited because the additional substitutions possibly result in a second phase. If the researchers can accurately obtain the stress along a certain axis, the piezoelectric properties in ABO_3 piezoelectric systems can be further optimized using the current basis. The sensitive stress directions for BaTiO_3 , KNbO_3 , and PZT(60/40) at room temperature are analyzed and discussed in the Supplemental Material [78]. A large number of pre-experiments should be tried and tested because it is difficult to achieve uniaxial compressive stress (rather than hydrostatic pressure) in a polycrystal via doping. According to the discussion in the present and previous results, the radius and valence of the substitution ion are two chief considerations because they determine the distribution of ions in the lattice [66–69]. In our opinion, stress-driven flattening of a free-energy profile will be a new research direction to obtain large piezoelectric response. The present study provides a promising route to the large piezoelectric effect induced by stress-driven flattening of a free-energy profile.

IV. CONCLUSIONS

In conclusion, the acceptor-donor codoping route can improve the piezoelectric performance of the tetragonal PZT system and BaTiO_3 . XRD analyses revealed that acceptor-donor substituting at A sites of ABO_3 ferroelectrics induces compressive stress along the $[001]_{\text{pc}}$ direction. Based on Landau-Ginzburg-Devonshire theory, the compressive stress results in the flattening of a free-energy profile in the PZT systems and BaTiO_3 . The flattening degree of a free-energy profile in the tetragonal PZT induced by doping is larger than that in the rhombohedral one, which is regarded as the reason why the enhanced effect of doping is significant in tetragonal PLAZT, but not in rhombohedral PLAZT. Differing from many reported experimental approaches (compositionally or temperature driven) for flattening of a free-energy profile, the method in this work is stress driven. The stress-driven flattening of a free-energy profile can continue to optimize the piezoelectric performance of ABO_3 systems on the basis of a compositionally driven one (the MPB).

ACKNOWLEDGMENTS

This work was financially supported by the National Natural Science Foundation of China (Grants No. 11272102, No. 51471057, and No. 51677033) and the Open Project of the Key Laboratory of Engineering Dielectrics and Its Application (Grant No. DJZ201401). The authors thank Dr. Shu-Ren Lin of the University of California, Berkeley, and Dr. Fei Zhou of the Harbin Institute of Technology for helpful discussions.

- [1] W. Hu *et al.*, *Nat. Mater.* **12**, 821 (2013).
- [2] X. J. Cheng, Z. W. Li, and J. G. Wu, *J. Mater. Chem. A* **3**, 5805 (2015).
- [3] W. Hu, K. Lau, Y. Liu, R. L. Withers, H. Chen, L. Fu, B. Gong, and W. Hutchison, *Chem. Mater.* **27**, 4934 (2015).
- [4] S. H. Ding, P. Zhao, T. X. Song, and X. J. Yang, *Ferroelectrics* **426**, 66 (2012).
- [5] S. H. Ding, T. X. Song, X. J. Yang, X. B. Liu, and G. B. Liu, *Ceram. Int.* **38**, S33 (2012).
- [6] D. Wu, B. Fang, Q. Du, and J. Ding, *Ferroelectrics* **432**, 81 (2012).
- [7] X. G. Zhao, P. Liu, Y. C. Song, A. P. Zhang, X. M. Chen, and J. P. Zhou, *Phys. Chem. Chem. Phys.* **17**, 23132 (2015).
- [8] M. Zhou, J. Zhang, L. Ji, Y. Wang, J. Wang, and F. Yu, *Ceram. Int.* **40**, 853 (2014).
- [9] T. H. Dinh, M. R. Bafandeh, J.-K. Kang, C.-H. Hong, W. Jo, and J.-S. Lee, *Ceram. Int.* **41**, S458 (2015).
- [10] C. Jullian, *J. Appl. Phys.* **95**, 4316 (2004).
- [11] M. Marsilius, K. G. Webber, E. Aulbach, and T. Granzow, *J. Am. Ceram. Soc.* **93**, 2850 (2010).
- [12] W. Liu, W. Chen, L. Yang, L. Zhang, Y. Wang, C. Zhou, S. Li, and X. Ren, *Appl. Phys. Lett.* **89**, 172908 (2006).
- [13] J. Li, X. Chai, D. Peng, H. Zou, X. Wang, and X. Yao, *Appl. Phys. Lett.* **105**, 082901 (2014).
- [14] D. Xu, W. L. Li, L. D. Wang, W. Wang, W. P. Cao, and W. D. Fei, *Acta Mater.* **79**, 84 (2014).
- [15] Y. Feng, W. L. Li, D. Xu, Y. L. Qiao, Y. Yu, Y. Zhao, and W. D. Fei, *ACS Appl. Mater. Interfaces* **8**, 9231 (2016).
- [16] Y. Feng, W. L. Li, D. Xu, W. P. Cao, Y. Yu, and W. D. Fei, *RSC Adv.* **6**, 36118 (2016).
- [17] J. L. Jones, E. Aksel, G. Tutuncu, T.-M. Usher, J. Chen, X. Xing, and A. J. Studer, *Phys. Rev. B* **86**, 024104 (2012).
- [18] Q. M. Zhang, H. Wang, N. Kim, and L. E. Cross, *J. Appl. Phys.* **75**, 454 (1994).
- [19] J. Gao, Z. Xu, F. Li, C. Zhang, Y. Liu, G. Liu, and H. He, *J. Appl. Phys.* **109**, 114111 (2011).
- [20] L. Fan, J. Chen, Y. Ren, Z. Pan, L. Zhang, and X. Xing, *Phys. Rev. Lett.* **116**, 027601 (2016).
- [21] F. Cordero, F. Trequattrini, F. Craciun, and C. Galassi, *Phys. Rev. B* **87**, 094108 (2013).
- [22] E. Buixaderas, D. Nuzhnyy, J. Petzelt, L. Jin, and D. Damjanovic, *Phys. Rev. B* **84**, 184302 (2011).
- [23] H. Guo, B. K. Voas, S. Zhang, C. Zhou, X. Ren, S. P. Beckman, and X. Tan, *Phys. Rev. B* **90**, 014103 (2014).
- [24] A. K. Kalyani, H. Krishnan, A. Sen, A. Senyshyn, and R. Ranjan, *Phys. Rev. B* **91**, 024101 (2015).
- [25] J. L. Zhang, X. J. Zong, L. Wu, Y. Gao, P. Zheng, and S. F. Shao, *Appl. Phys. Lett.* **95**, 022909 (2009).
- [26] N. Ma, B. P. Zhang, W. G. Yang, and D. Guo, *J. Eur. Ceram. Soc.* **32**, 1059 (2012).
- [27] R. E. Cohen and H. Fu, *Nature (London)* **403**, 281 (2000).
- [28] J. Gao *et al.*, *Appl. Phys. Lett.* **107**, 032902 (2015).
- [29] K. Brajesh, K. Tanwar, M. Abebe, and R. Ranjan, *Phys. Rev. B* **92**, 224112 (2015).
- [30] K. Wang and J. F. Li, *Adv. Funct. Mater.* **20**, 1924 (2010).
- [31] B. Noheda, D. E. Cox, G. Shirane, R. Guo, B. Jones, and L. E. Cross, *Phys. Rev. B* **63**, 014103 (2000).
- [32] W. F. Liu and X. B. Ren, *Phys. Rev. Lett.* **103**, 257602 (2009).
- [33] M. Porta and T. Lookman, *Phys. Rev. B* **83**, 174108 (2011).
- [34] R. S. Solanki, S. K. Mishra, Y. Kuroiwa, C. Moriyoshi, and D. Pandey, *Phys. Rev. B* **88**, 184109 (2013).
- [35] K. Wang, F. Z. Yao, W. Jo, D. Gobeljic, V. V. Shvartsman, D. C. Lupascu, J. F. Li, and J. Rodel, *Adv. Funct. Mater.* **23**, 4079 (2013).
- [36] Y. Ishibashi and M. Iwata, *Jpn. J. Appl. Phys.* **37**, L985 (1998).
- [37] Y. Ishibashi and M. Iwata, *Jpn. J. Appl. Phys.* **38**, 1454 (1999).
- [38] M. Iwata and Y. Ishibashi, *Jpn. J. Appl. Phys.* **39**, 5156 (2000).
- [39] M. Iwata and Y. Ishibashi, *Jpn. J. Appl. Phys.* **38**, 5670 (1999).
- [40] D. Damjanovic, *J. Am. Ceram. Soc.* **88**, 2663 (2005).
- [41] M. Budimir, D. Damjanovic, and N. Setter, *J. Appl. Phys.* **94**, 6753 (2003).
- [42] M. Budimir, D. Damjanovic, and N. Setter, *Phys. Rev. B* **72**, 064107 (2005).
- [43] M. Davis, M. Budimir, D. Damjanovic, and N. Setter, *J. Appl. Phys.* **101**, 054112 (2007).
- [44] D. Damjanovic, M. Budimir, M. Davis, and N. Setter, *J. Mater. Sci.* **41**, 65 (2006).
- [45] M. Gröting and K. Albe, *Phys. Rev. B* **89**, 054105 (2014).
- [46] J. Gao, F. Li, Z. Xu, C. Zhang, Y. Liu, G. Liu, T. Zhang, and H. He, *J. Phys. D: Appl. Phys.* **46**, 215304 (2013).
- [47] L. Bellaiche, A. García, and D. Vanderbilt, *Phys. Rev. B* **64**, 060103 (2001).
- [48] M. Ahart *et al.*, *Nature (London)* **451**, 545 (2008).
- [49] M. Matsubara, T. Yamaguchi, W. Sakamoto, K. Kikuta, T. Yogo, and S. Hirano, *J. Am. Ceram. Soc.* **88**, 1190 (2005).
- [50] H. B. Yang, C. R. Zhou, X. Y. Liu, Q. Zhou, G. H. Chen, W. Z. Li, and H. Wang, *J. Eur. Ceram. Soc.* **33**, 1177 (2013).
- [51] B. Noheda, J. A. Gonzalo, L. E. Cross, R. Guo, S. E. Park, D. E. Cox, and G. Shirane, *Phys. Rev. B* **61**, 8687 (2000).
- [52] A. K. Singh, D. Pandey, S. Yoon, S. Baik, and N. Shin, *Appl. Phys. Lett.* **91**, 192904 (2007).
- [53] D. Damjanovic, *Appl. Phys. Lett.* **97**, 062906 (2010).
- [54] M. Budimir, D. Damjanovic, and N. Setter, *Phys. Rev. B* **73**, 174106 (2006).
- [55] Y. Tian, L. Wei, X. Chao, Z. Liu, and Z. Yang, *J. Am. Ceram. Soc.* **96**, 496 (2013).
- [56] T. Yamamoto, *Jpn. J. Appl. Phys.* **35**, 5104 (1996).
- [57] X. B. Ren, *Nat. Mater.* **3**, 91 (2004).
- [58] L. P. Hu, T. J. Zhu, X. H. Liu, and X. B. Zhao, *Adv. Funct. Mater.* **24**, 5211 (2014).
- [59] A. V. Kimmel, P. M. Weaver, M. G. Cain, and P. V. Sushko, *Phys. Rev. Lett.* **109**, 117601 (2012).
- [60] A. Chandrasekaran, D. Damjanovic, N. Setter, and N. Marzari, *Phys. Rev. B* **88**, 214116 (2013).
- [61] Z. Feng and X. Ren, *Phys. Rev. B* **77**, 134115 (2008).
- [62] L. Gao, Y. Huang, Y. Hu, and H. Du, *Ceram. Int.* **33**, 1041 (2007).
- [63] L. Gao, Y. Huang, L. Liu, T. Liu, C. Liu, F. Zhou, and X. Wan, *J. Mater. Sci.* **43**, 6267 (2008).
- [64] Y. Huang, L. Gao, Y. Hu, and H. Du, *J. Mater. Sci.: Mater. Electron.* **18**, 605 (2007).
- [65] M. Rawat and K. L. Yadav, *Ceram. Int.* **39**, 3627 (2013).
- [66] N. Setter and L. E. Cross, *J. Appl. Phys.* **51**, 4356 (1980).
- [67] N. Setter and L. E. Cross, *J. Mater. Sci.* **15**, 2478 (1980).
- [68] F. Fei and Z. Xiaowen, *Ferroelectrics* **197**, 67 (1997).
- [69] G. King, E. Goo, T. Yamamoto, and K. Okazaki, *J. Am. Ceram. Soc.* **71**, 454 (1988).

- [70] R. D. Shannon, *Acta Crystallogr., Sect. A* **32**, 751 (1976).
- [71] W. Ge, C. P. Devreugd, D. Phelan, Q. Zhang, M. Ahart, J. Li, H. Luo, L. A. Boatner, D. Viehland, and P. M. Gehring, *Phys. Rev. B* **88**, 174115 (2013).
- [72] D. K. Khatua, K. V. Lalitha, C. M. Fancher, J. L. Jones, and R. Ranjan, *Phys. Rev. B* **93**, 104103 (2016).
- [73] M. J. Haun, E. Furman, S. J. Jang, and L. E. Cross, *Ferroelectrics* **99**, 13 (1989).
- [74] M. J. Haun, E. Furman, S. J. Jang, and L. E. Cross, *Ferroelectrics* **99**, 63 (1989).
- [75] M. J. Haun, E. Furman, S. J. Jang, H. A. McKinstry, and L. E. Cross, *J. Appl. Phys.* **62**, 3331 (1987).
- [76] M. J. Haun, E. Furman, H. A. McKinstry, and L. E. Cross, *Ferroelectrics* **99**, 27 (1989).
- [77] N. A. Pertsev, A. G. Zembilgotov, and A. K. Tagantsev, *Phys. Rev. Lett.* **80**, 1988 (1998).
- [78] See Supplemental Material at <http://link.aps.org/supplemental/10.1103/PhysRevMaterials.1.064405> for the stress dependence of the elastic Gibbs free energy profile with respect to spontaneous polarization, the effect of compressive stress on polarization rotation, the compressive stress in the rhombohedral PZT(60/40), and the sensitive stress direction for BaTiO₃, KNbO₃, and PZT(60/40).
- [79] Z. G. Wu and R. E. Cohen, *Phys. Rev. Lett.* **95**, 037601 (2005).
- [80] P. E. Janolin, P. Bouvier, J. Kreisel, P. A. Thomas, I. A. Kornev, L. Bellaiche, W. Crichton, M. Hanfland, and B. Dkhil, *Phys. Rev. Lett.* **101**, 237601 (2008).
- [81] J. Rouquette, J. Haines, V. Bornand, M. Pintard, P. Papet, C. Bousquet, L. Konczewicz, F. A. Gorelli, and S. Hull, *Phys. Rev. B* **70**, 014108 (2004).
- [82] A. Sani, B. Noheda, I. A. Kornev, L. Bellaiche, P. Bouvier, and J. Kreisel, *Phys. Rev. B* **69**, 020105 (2004).
- [83] S. H. Oh and H. M. Jang, *Ceram. Int.* **26**, 565 (2000).
- [84] J. Rouquette, J. Haines, G. Fraysse, A. Al-Zein, V. Bornand, M. Pintard, P. Papet, S. Hull, and F. A. Gorelli, *Inorg. Chem.* **47**, 9898 (2008).
- [85] J. Kreisel, B. Noheda, and B. Dkhil, *Phase Transit.* **82**, 633 (2009).
- [86] J. Rouquette, J. Haines, V. Bornand, M. Pintard, P. Papet, and F. A. Gorelli, *J. Eur. Ceram. Soc.* **25**, 2393 (2005).
- [87] M. Hinterstein, J. Rouquette, J. Haines, Ph. Papet, M. Knapp, J. Glaum, and H. Fuess, *Phys. Rev. Lett.* **107**, 077602 (2011).
- [88] M. Hinterstein, J. Rouquette, J. Haines, Ph. Papet, J. Glaum, M. Knapp, J. Eckert, and M. Hoffman, *Phys. Rev. B* **90**, 094113 (2014).
- [89] M. Hinterstein, M. Hoelzel, J. Rouquette, J. Haines, J. Glaum, H. Kungl, and M. Hoffman, *Acta. Mater.* **94**, 319 (2015).
- [90] C. Y. Wu, W. H. Duan, X. W. Zhang, and Z. R. Liu, *J. Appl. Phys.* **108**, 124102 (2010).